Nuclear Instruments and Methods in Physics Research A 728 (2013) 73–80

Contents lists available at SciVerse ScienceDirect

Nuclear Instruments and Methods in Physics Research A

journal homepage: www.elsevier.com/locate/nima

Spectral identification of a ^{90}Sr source in the presence of masking nuclides using Maximum-Likelihood deconvolution

Marcus J. Neuer *

VDEh Betriebsforschungsinstitut, Sohnstr. 65, 40237 Duesseldorf, Germany

ARTICLE INFO

Article history:
Received 9 April 2013
Received in revised form
17 May 2013
Accepted 5 June 2013
Available online 17 June 2013

Keywords:
Beta minus
Nuclide identification
Deconvolution
Maximum-Likelihood
Strontium

ABSTRACT

A technique for the spectral identification of strontium-90 is shown, utilising a Maximum-Likelihood deconvolution. Different deconvolution approaches are discussed and summarised. Based on the intensity distribution of the beta emission and Geant4 simulations, a combined response matrix is derived, tailored to the β^- detection process in sodium iodide detectors. It includes scattering effects and attenuation by applying a base material decomposition extracted from Geant4 simulations with a CAD model for a realistic detector system. Inversion results of measurements show the agreement between deconvolution and reconstruction. A detailed investigation with additional masking sources like ^{40}K, ^{226}Ra and ^{131}I shows that a contamination of strontium can be found in the presence of these nuisance sources. Identification algorithms for strontium are presented based on the derived technique. For the implementation of blind identification, an exemplary masking ratio is calculated.

1. Introduction

The last decade has seen several novel technologies for spectrum analysis, driven mostly by the evolving requirements of both nuclear security and safety. Challenged by a rising threat of nuclear terrorism, the security branch seeks for a variety of instruments that can be handled by more or less untrained personnel to perform different tasks of nuclear inspections. Additionally, with the recent events of the reactor incident at the Fukushima plant, Japan, a series of important safety considerations was brought back into the focus of the nuclear physics community.

Still, there is a high demand for reliable technologies that provide an automatised and correct threat announcement once radioactive emissions are detected. The decision whether a source is considered as threat or not is based on an investigation of the radiations isotopic composition, usually performed by analysing its spectroscopic fingerprints. As a rather complex procedure, the latter requires detailed knowledge of the associated spectra and is mostly mastered by experts specialised in this field. Of course, it is necessary to provide automated detection and identification tools to border securing officers, firefighters and police squads, as to mention just a few examples of user groups that cannot be trained to become experts in spectral analysis in addition to their own important set of skills. Here, it is crucial to map the expert knowledge into algorithmic schemes to assist the personnel with its tasks at hand.

For all these radiation analysis products the key idea is to deter the user from the issues and complexity of the detection and analysis process itself and to keep most of the physical core tasks, including the identification, hidden as a black box. Algorithms were developed to learn and identify sources based on their spectral shape and commercial detection products exist that are designed specifically for the identification of nuclear sources.

Furthermore, in the field of food and contamination analysis, those technologies play an increasingly relevant role. With the fallout from nuclear accidents affecting rural and farming areas dedicated to the cultivation of nutrition, it becomes necessary to carefully observe the world-wide cargo routes with specialised equipment. As of today, such evaluations are done by laboratories with dedicated instruments, food monitors, that are commonly fed with piecewise tests of food samples. Caused by the Fukushima incident, vast amounts of ^{137}Cs, ^{131}I, ^{132}Te and ^{90}Sr contaminated large rural areas around the plant. The short living isotopes as ^{131}I, having a half life of about 8 days or ^{132}Te with 3.2 days quickly vanished, leaving the long-living isotopes ^{137}Cs with 30 years and ^{90}Sr with 28 years as the main contributions.

But not all nuclides are equally important and a group of around forty sources can be regarded as highly relevant, nearly all of which feature a distinct γ-pattern. Modern equipment is more or less able to identify these sources and there are standards for nuclear security, Ref. [1] is just one example, specifying an exact list of nuclides that is desired to be found.

In nearly all scenarios stated above, the strontium isotope ^{90}Sr is an exception. After the first nuclear tests and their world wide

* Tel.: +49 175 2064672.
E-mail address: marcus.neuer@mndevelopments.de

0168-9002/$ - see front matter © 2013 Elsevier B.V. All rights reserved.
http://dx.doi.org/10.1016/j.nima.2013.06.013

fallout, a number of works [2,3] investigated its impact on biological material and way to determine its concentration in essential nutrition products like milk [4]. From the scintillation perspective, strontium yields a very decisive problem: it is a β^- emitter and when measured with e.g. a sodium iodide scintillation detector, it produces a continuous spectrum that has no characteristic peaks. For most algorithms this fact leads to the difficulty to identify ^{90}Sr correctly, especially if it is masked by nuisance isotopes. As a matter of fact, the identification of strontium in a simple, algorithmic way using low-cost equipment for its detection is very desirable and, as we already briefly discussed, many types of nuclear equipment could be significantly improved by it. Any subsequent threat categorisation [5] would benefit from such a solution.

In the course of this work, we will consequently focus on ^{90}Sr and present such an algorithm that identifies its continuous radiation even in the presence of masking sources. Threat isotopes emit γ-radiation with distinct peak pattern. More or less all algorithms somehow deduce their result from the peak pattern, either by locating the peaks and intensities or simply by matching the whole shape with the reference data. Without neglecting that germanium semi-conductor detectors provide probably the most accurate spectroscopic quality in terms of resolution and offer a high precision analysis of the radiation, our method is specifically designed to sodium iodide scintillator detectors, because they are a workhorse in the nuclear detection industry, cheaper and far more widely distributed than the high-resolving germanium.

We will describe a procedure that discovers the ^{90}Sr source based on response modelling and likelihood maximisation. Using the original distribution function of β^- emitters, we will construct a generalised response matrix, the so-called endpoint matrix that combines the unique features of the β^-.

The procedure will identify the continuous contributions of a β^- source in a bare and slightly shielded configuration and in the presence of other sources, explicitly considering the masking with strongly scattered sources. While we focus on the isotope ^{90}Sr, the method remains applicable for other β^- sources, too. We do not intend to distinguish between multiple β^- materials. Note that shielding has an enormous influence on the shape of the strontium spectrum, because its most characteristic counts are detected in the first hundred channels. Our model includes an average shielding that shows good results for the low and medium shielded cases.

Our document is structured as follows: after this short introduction we will present a brief summary of spectral deconvolution techniques in Section 2, beginning with their relevance in the context of other publications and concluding with the formal statement of the Maximum-Likelihood expectation maximisation (MLEM). As the latter algorithm requires the knowledge of the so-called response matrix, Section 3 will deal with the derivation of a β^- specific response model and its inclusion in the MLEM algorithm. The final deconvolution has been tested with ^{90}Sr and masking sources in Section 4. Section 5 gives an overview of the application of our deconvolution technique as identification algorithm for ^{90}Sr. Here, the unique characteristics of the deconvolved solution are used to establish a decision threshold. Finally Section 6 yields an outlook on upcoming applications and extensions of our algorithm.

2. Maximum-Likelihood deconvolution of γ-spectra

In this section we will concentrate on the question, how far the impact of certain physical interactions that define spectrum characteristics can in fact be mathematically reversed by a procedure which is called deconvolution or sometimes simply inversion. As the name already suggests, the nature of the interactions is restricted to systems where the complete answer function is produced by convolving responses of the subprocesses.

Original roots of inversion equations can be found in the prominent geological discipline of seismic exploration, where in 1954 Robinsion [6] presented a way for predictions based on the decomposition of time series, heavily inspired by the fundamental works by Wiener during that time.

Deconvolution is a longstanding topic in spectrum analysis and has also been discussed in the literature for quite a while. From the emission of radiation to the spectral acquisition, multiple physical processes like material absorption, the photo effect inside a detector or the Compton-scattering take place and for our following concept we assume that these steps can be reversed for a given source. Spectral deconvolution was indeed thoroughly reviewed by Bouchet [7] in 1995, comparing different deconvolution techniques and summarising their advantages and disadvantages. The conclusion of his work pointed already towards two rather similar algorithms, one based on an iterative maximisation of a likelihood estimator and the other applying an iterative entropy maximisation, both turning out to have significant potential for use in the spectrum analysis domain.

A-priori knowledge is the fundamental input of the deconvolution and in the context of spectrum deconvolution this is given in terms of the detectors response. The latter can be modelled by a matrix that relates the incoming energies (that hit the detector) with the output spectrum. A short illustrative introduction on these matrices is given in the next section.

In a rigorous application related approach, Meng and Ramsden [8] revisited three of these algorithms to investigate possible benefits for a virtual resolution improvement of low-cost scintillators like cesium iodide or sodium iodide. They explored the possibilities of symmetric detector concepts, leveraging the benefits of a homogenous response matrix and their processed spectra featured much sharper peaks, making the spectra easier to interpret by eye or by algorithmic means. As a main result, they provided evidence that the Maximum-Likelihood technique is superior to its alternatives and appears to be the method of choice for spectrum deconvolution tasks.

With the market requesting cheaper radiation detection equipment, development activities went towards plastic scintillators, having a remarkable sensitivity for radiation but unfortunately a very low intensity of the photo-peaks. For most of their energy ranges, they feature a purely continuous spectrum that is dominated by a smooth, edge-like structure produced by Compton-scattering. Response matrices were calculated for these extreme types of spectra and it is possible to virtually reconstruct the photo-peaks with astonishing quality, as e.g. discussed by Butchins et al. [9].

The deconvolution of plastic spectra shows in principle that continuous spectra and continuous responses are suitable to perform a stable inversion. Consequently it is also possible to unfold other continuous spectra, as in our case produced by β^- emitters, as well.

The way the deconvolution methods work can be easily understood as follows: the original spectrum of a radioactive source – as the experimental result – is a projection onto a given discrete channel space. Once a relationship between the incident energy and the out coming spectrum is established – mathematically this relationship is the response matrix – an inversion can be calculated that maps the measurement back on the incident energies. The decisive point is that, while the measurement as such always contains the information core, the deconvolution matrix and the subsequent inversion represent a defined scheme by which information is interpreted. In other words, the deconvolution reduces the solution space to the most-likely solutions which must be known a-priori for a given detector.

2.1. Construction of the detector response matrix

In previous works, response matrices for γ-detection have been successfully applied to various problems, as shown e.g.

by Estep et al. [10] and Wilderman et al. [11]. Lately, Herbach et al. [12] showed a convenient way to rapidly generate spectra from these responses without re-running complex Monte-Carlo codes like e.g. Geant4 [13] multiple times and we will focus on this kind of simulation, because it helps to understand the way the response matrix framework can be extended to β^- responses later. We first split the simulation process into smaller modules for each physical stage:

(1) *Emission*: Based on the ENSDF data, the decay chain data and data about important source groups. The emission is typically described by some table
$$\mathcal{I}_\gamma = \mathcal{I}_\gamma(E) \tag{1}$$
mapping the emission lines at energies E to the observed intensities $\mathcal{I}$, which is of course the central input when you deal with distinct γ-lines. For our purposes, we used a nuclear decay database (ENSDF, http://www-nds.iaea.org/nsdd/) containing these tables. In the case of pure β^- sources, it contains the so-called endpoint energy Q.

(2) *Material interaction*: Material interacts with the radiation in the source material by self-absorption in the space between the source and the detector and inside the detector. It was shown in a series of works [10,14,15] that an attenuation A can be efficiently approximated by a linear combination, using a suitable set of material base functions α_i:
$$A(E) = \sum_i w_i \alpha_i(E). \tag{2}$$
A detailed list of our material base functions $\alpha_i(E)$ can be found in Appendix A.

(3) *Raw detector response*: This matrix describes the physics of the detection process, but explicitly not the statistical processes that are responsible for the peak broadening. It is generated by Monte-Carlo simulation with Geant4 [13] using mono-energetic line energies and a CAD model of the full mechanical assembly. After generating lists of the deposited energies, we histogram these energies and get the idealised detector response
$$\mathbf{D} = \begin{pmatrix} D_1(E_1) & D_2(E_1) & \cdots & D_N(E_1) \\ D_1(E_2) & D_2(E_2) & \cdots & D_N(E_2) \\ \cdots & \cdots & \cdots & \cdots \\ D_1(E_N) & D_2(E_N) & \cdots & D_N(E_N) \end{pmatrix}, \tag{3}$$
which relates each i-th incoming energy with a spectrum given by $D_i(E)$.

(4) *Resolution and statistics*: Resolution of a spectrum depends on multiple processes inside the detector assembly and on the signal processing within the read-out electronics. For our purpose, we simply measure the resolution dependency of our detector with respect to certain γ-peaks, approximating the resolution vs. energy curve,
$$\rho = \rho(E), \tag{4}$$
yielding a mean to fold our artificial spectra with the correct resolution. Both the use of the raw detector response and the assessment of the resolution function were treated in Ref. [16] by Römer et al. in some detail.

Summarising, the emission spectrum $\mathcal{I}_\gamma(E)$ is generated from the ENSDF, folded with a material function $A(E)$, which is composed of our material base functions, then folded with the detector response matrix $\mathbf{D}$ and folded with the detector specific, experimentally accessed resolution model $\rho(E)$: with this procedure $\mathcal{P}$, we can finally simulate spectra
$$\zeta(E) = \mathcal{P}[\mathcal{I}_\gamma(E); A(E), \mathbf{D}, \rho(E)], \tag{5}$$
for arbitrary input energies, containing all relevant physical interactions that a given gamma quant will experience on its way from the source to the detector, where it finally produces a photo-absorption, a Compton-scattering or simply an escape event.

In our case all four steps for the procedure $\mathcal{P}$ are conveniently implemented in a Matlab framework and allow for the simulation of model spectra from unaccessible sources, as e.g. plutonium or uranium, including the statistical individuality of a specific detector system. Similar simulation frameworks have been already integrated into the production of nuclear surveillance equipment as shown in Refs. [12,17].

As a last step, we identify the complete detector response matrix $\mathbf{R}$, which is simply the input of mono-energetic lines – again – into the whole simulation process
$$\mathbf{R} = \mathcal{P}[\mathbf{1}; A(E), \mathbf{D}, \rho(E)]. \tag{6}$$

Fig. 1 shows an illustration of this matrix for the specific case of material No. 5, the raw detector response of a 2 in. by 4 in. sodium iodide detector and its individual response curve $\rho(E)$ accessed by measurements. Each column represents the event spectrum of a mono-energetic line incident energy, in our case a range from 3 keV to 3072 keV separated with discrete energies of $\Delta E = 3$ keV, thus giving us a 1024×1024 matrix. All spectroscopic features are represented within the matrix, including the photo peak on the main diagonal followed by the Compton-edge. Consistently, both escape peaks appear when the incident energy becomes greater than 1022 keV.

2.2. Response inversion

A measured spectrum μ can be described in a simplified form:
$$\mu(E) = \sum_E' R(E, E')\varphi(E') + \varepsilon_{E'}, \tag{7}$$
with the incident energies φ hitting the detector. ε is a noise or perturbation term that represents the intrinsic difference between the reality and the model or as Bouchet terms it in [7], the incompleteness of the reference. The latter equation can be also written in vectorial form
$$\mu = \mathbf{R}\,\varphi + \varepsilon, \tag{8}$$
and in an idealised case $\varepsilon = 0$ this would straightforwardly lead to the inversion
$$\varphi = \mathbf{R}\backslash\mu, \tag{9}$$
and therefore to a determination of the incident spectrum φ. With

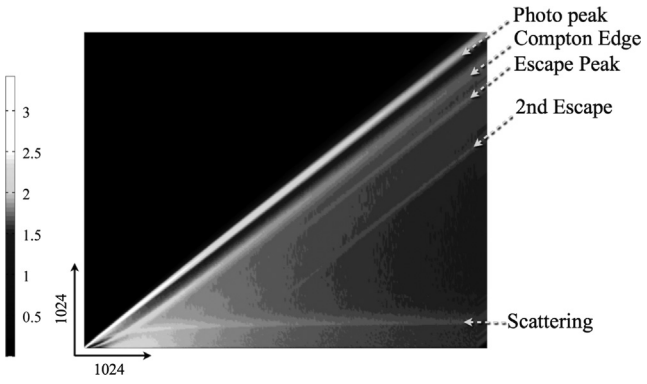

Fig. 1. Example of a full detector response function $\mathbf{R}$ for a 2 in. by 4 in. sodium iodide detector: each column represents the spectrum of a virtual, mono-energetic line emission. The picture shows the combination of a material $A(E)$, in this case 1 mm cadmium shielding, the raw detector response $\mathbf{D}$ and the resolution function $\rho(E)$.

the rather realistic condition $\varepsilon \neq 0$, the situation becomes more complicated and the discussions of that case originated in many different fields, Subrahmanya [18] or Suyu et al. [19] are just two examples of such works. The common way to find φ for $\varepsilon \neq 0$ is by minimising the χ^2 expression

$$\chi^2 = (\mu - \mathbf{R}\varphi)^T \mathbf{C}_\varepsilon^{-1} (\mu - \mathbf{R}\varphi) \tag{10}$$

under consideration of the covariance matrix $\mathbf{C}$. Most direct solutions based on Eq. (10) proved unsuccessful due to their sensitivity to noise. Following the conclusions of Bouchet, Meng and Ramsden, one method is exceptionally useful to solve the above described inversion step: the Maximum-Likelihood expectation maximisation (MLEM) which was presented in the works of Shepp and Vardi in 1982 [20]. This procedure is principally different, because it is iterative: it starts with an a-priori assumption of the solution $\varphi^{(0)}$ and converges into the complete inversion with each successive iteration step, calculated by

$$\varphi_i^{(\alpha+1)} = \varphi_i^{(\alpha)} \sum_{j=0}^{M} \frac{\mu_j R_{i,j}}{\sum_k \varphi_k^{(\alpha)} R_{k,j}}. \tag{11}$$

Here, $M = 1024$ reflect the dimension of the response matrix, $\alpha = 1, \ldots, N$ is the number of the iteration and N refers to the maximum amount of iterations that is used in Eq. (11). Note that we still have the freedom to choose the initial distribution $\varphi^{(0)}$.

For sufficiently large α, $\varphi^{(\alpha)}$ converges into a vector such that $\mathbf{R}\varphi^{(\alpha)}$ becomes close to μ,

$$\lim_{\alpha \to \infty} [(\mu - \mathbf{R}\varphi^{(\alpha)})^T \mathbf{C}_\varepsilon^{-1} (\mu - \mathbf{R}\varphi^{(\alpha)})] \approx 0 \tag{12}$$

We denote the evaluation of Eq. (11) as deconvolution of the measured spectrum μ with the response matrix $\mathbf{D}$ and abbreviate it with the symbol $\mathcal{D}$,

$$\varphi = \mathcal{D}(\mu, \mathbf{R}, N, \varphi^{(0)}). \tag{13}$$

3. Deconvolution of continuous β^- spectrum parts

To apply the presented MLEM deconvolution technique in the case of continuous spectra from β^- sources, we need to perform two steps:

(A) Generate a physically correct emission matrix for the β^- process, and
(B) integrate this emission matrix into step (1) of Section 2.1 to combine it with $A(E)$, $\mathbf{D}$ and $\rho(E)$ to a β^- response matrix $\mathbf{R}_{\beta^-}$ using Eq. (6).

3.1. Energy distribution of the β^- emission

Next, we state a mechanism that produces adequate β^- emission spectra, denoted with $\mathcal{I}_{\beta^-}(E)$. The latter is a well-known part of the original description of the β-decay, whose energy distribution can be derived following textbooks on nuclear radiation as e. g. [21]: first, we abbreviate the relativistic impulse

$$\kappa = \sqrt{(m_e c^2 + E)^2 - m_e^2 c^4} \tag{14}$$

where m_e is the mass of an electron and c is the speed of light in vacuum. Let $\mathcal{E}$ be defined as a rescaled energy,

$$\mathcal{E} = 2\pi Z \alpha \frac{(m_e c^2 + E)}{\kappa}, \tag{15}$$

with the atomic number Z and the fine structure constant $\alpha = 1/137$, then the distribution of the β^- energies is given in terms of

$$\mathcal{I}_{\beta^-}(E, Q) = \frac{\mathcal{E}(E)}{1 - \exp[-\mathcal{E}(E)]} [m_e c^2 + E][Q - E]^2 \kappa. \tag{16}$$

3.2. Endpoint emission matrix

As we have shown in the previous section, we have a straightforward way to generate spectra, especially for β^- spectra and we will use this framework to construct the so-called endpoint (response) matrix.

For each endpoint energy Q_i we calculate (a) the emission spectrum $\mathcal{I}_{\beta^-}(E, Q_i)$ and (b) the final simulation $\mathcal{P}[\Delta(E, Q_i); A(E), \mathbf{D}, \rho(E)]$, thus generating a matrix that relates the endpoint energies with their associated emission spectra

$$\mathbf{B} = \begin{pmatrix} \mathcal{I}_{\beta^-}(E_1, Q_1) & \mathcal{I}_{\beta^-}(E_1, Q_2) & \cdots & \mathcal{I}_{\beta^-}(E_1, Q_N) \\ \mathcal{I}_{\beta^-}(E_2, Q_1) & \mathcal{I}_{\beta^-}(E_2, Q_2) & \cdots & \mathcal{I}_{\beta^-}(E_2, Q_N) \\ \cdots & \cdots & \cdots & \cdots \\ \mathcal{I}_{\beta^-}(E_N, Q_1) & \mathcal{I}_{\beta^-}(E_N, Q_2) & \cdots & \mathcal{I}_{\beta^-}(E_N, Q_N) \end{pmatrix}, \tag{17}$$

whereas the spectra seen by our detector are

$$\zeta_{\beta^-}(E) = \mathcal{P}[\mathcal{I}_{\beta^-}(E, Q_i); A(E), \mathbf{D}, \rho(E)]. \tag{18}$$

Fig. 2 shows an example of the artificial emission simulation using Eq. (18) and its comparison with a real strontium measurement. For the calculation we used shielding function A_5 from the table included in the Appendix.

3.3. β^- response matrix

With the endpoint emission matrix, we can construct a β^- response matrix by Eq. (6), yielding

$$\mathbf{R}_{\beta^-} = \mathcal{P}[\mathbf{B}; A(E), \mathbf{D}, \rho(E)]. \tag{19}$$

Note that our processing chain strictly keeps the physical subprocesses in its correct order, first the emission of radiation, followed by absorption between the detector and the source and finally the detection. This is a crucial point, because simply folding the matrices $\mathbf{R}$ from Eq. (6) with $\mathbf{B}$ will not work, as the process chain would be re-ordered so that the emission takes place as last subprocess, which would be unphysical.

3.4. Inversion and reconstruction

In the next step we take the measurement of ^{90}Sr and deconvolve it using matrix $\mathbf{R}_{\beta^-}$. In Fig. 2 the measurement spectrum is presented and Fig. 3 yields the result of a $N = 500$ iteration deconvolution with

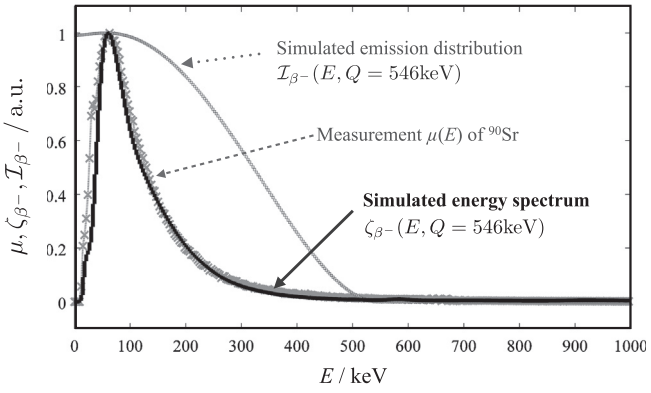

Fig. 2. Comparison of the artificial spectrum generated by Eq. (18) and a test measurement μ of strontium (1 μSv/h), acquired for 100 s with a 2 in. by 4 in. sodium iodide detector. The emission spectrum as calculated by Eq. (16) is shown in grey. All functions were normalised to their maximum.

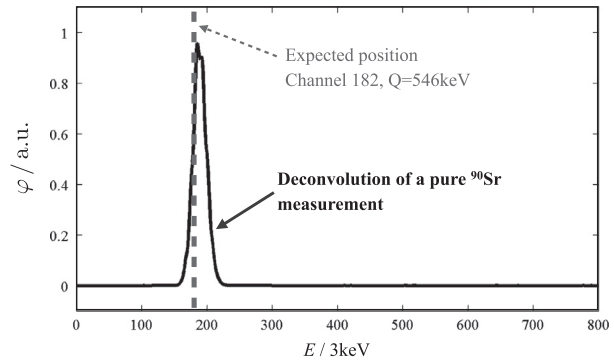

Fig. 3. Deconvolution φ of a ^{90}Sr measurement. The original measurement spectrum is shown in Fig. 2. Caused by the inversion process, a peak appears around channel 188 which is rather close to the expected value of the endpoint energy $Q=546$ keV≡182ch. $N=500$ iterations were used in this example.

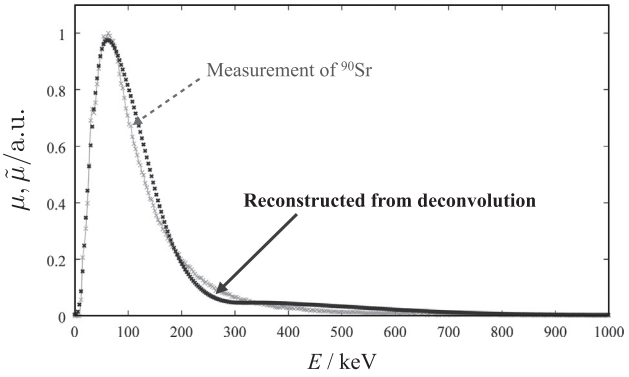

Fig. 4. Reconstruction $\tilde{\mu}$ of the spectrum by applying Eq. (21) to the deconvolution spectrum φ is shown in Fig. 3. For better comparison, we included the measured spectrum from Fig. 2, too.

the response matrix $\mathbf{R}_{\beta^-}$. Note the proximity and agreement of this (rather ideal) solution to the theoretic prediction. The deconvolution is established with Eq. (13) and a short transformation of our input data

$$\varphi = \mathcal{D}[\mu - \langle\mu\rangle, \mathbf{R} - \langle\mathbf{R}\rangle, N, \varphi^{(0)} - \langle\varphi^{(0)}\rangle], \tag{20}$$

where $\langle . \rangle$ brackets represent the calculation of the expectation value. The transformation can be regarded as a regularisation for the stability of the inversion. The reconstruction reverses this process and is given by

$$\tilde{\mu} = \mathbf{R}_{\beta^-}\varphi. \tag{21}$$

In Fig. 4 we show the reconstruction result, in order to check the consistency of our procedure. The agreement between the reconstructed spectrum with the original measurement is an important indicator of the quality of our response matrix. Still, some minor deviations from the measurement can be seen.

4. Results of ^{90}Sr masking scenarios

Our test of the deconvolution is a hybrid approach between measurement and a Monte-Carlo reduction of base spectra, closely following the procedure proposed in [22]. Our measurements were done by using long time acquisitions of potassium, radium and iodine and a subsequent downscaling to a defined real-time. As a detector we used a 2 in. by 4 in. food monitor system. Two major types of sources are of interest in our case: (a) strongly scattered sources and (b) multi-peak γ sources.

4.1. Masking with ^{40}K fertiliser

Our first test is done with ^{40}K to verify the technique with a source that produces an increased amount of scattering events in the sodium iodide detector. Potassium is part of the natural occurring radiation (NORM) widely used in fertiliser materials. Some exemplary spectra we tested are shown in Fig. 5, yielding the original pure fertiliser characteristic and a combination of this source with an amount of ≈0.2 μSv/h of strontium. The deconvolution results of both are found in Fig. 6. The spectrum with the small amount of strontium clearly shows the deconvolution peak close to the theoretical prediction at channel 182. Furthermore, both peaks clearly separate and can be used for an algorithmic decision for the presence of strontium.

4.2. Masking with strongly scattered ^{131}I

Iodine was one of the crucial parts of the Fukushima fall-out and though it has a very short half-life it is an important example, because it is widely used for medical purposes [17]. As a matter of fact, the source is frequently found to be incorporated by patients that have a certain kind of treatment. The human body must be regarded as a strong scatterer for radiation and therefore, iodine samples are typically tested with a polyethylene shielding that emulates the scattering effect of human tissue. This assumption is also more realistic for food samples, as we expect the source as such covered by the food substance.

Fig. 7 presents the pure original spectrum together with additional strontium contributions and Fig. 8 yields the actual deconvolution. Note the severe distortion of the spectral shape

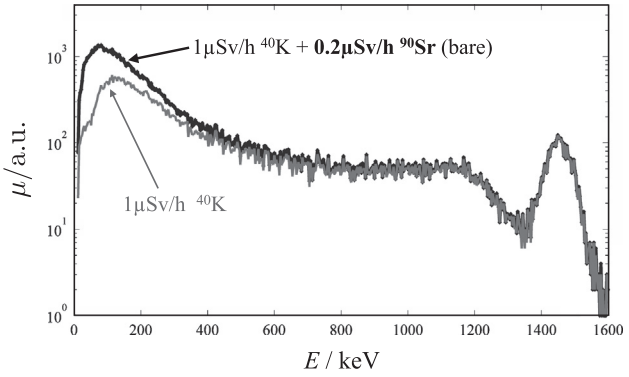

Fig. 5. Potassium as masking source for ^{90}Sr, using 1 μSv/h ^{40}K and 0.2 μSv/h ^{90}Sr. The strontium sources only add counts within the first 182 channels, ending with its endpoint energy of $Q=546$ keV.

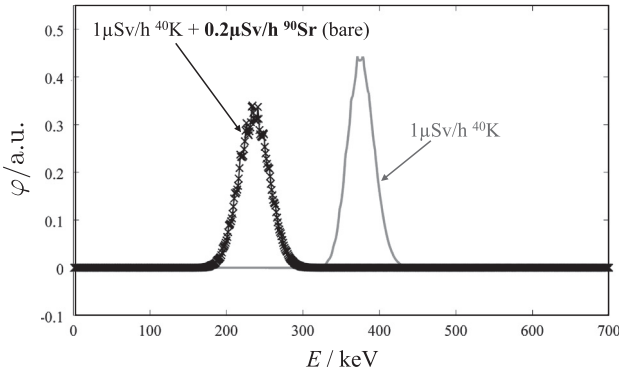

Fig. 6. Deconvolution of pure ^{40}K as shown in Fig. 5 compared against the deconvolution of ^{40}K masking ^{90}Sr. The iterations were fixed to $N=500$.

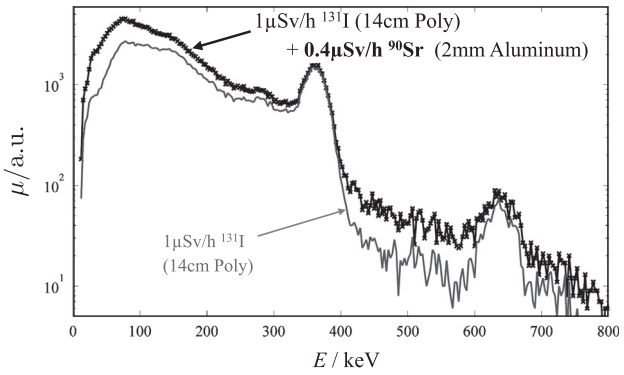

Fig. 7. Spectra of an iodine source with 1 μSv/h that were shielded with 14 cm of polyethylene to model a liquid emitter or a source enclosed in food. The pure source is marked in black and the iodine source with additional strontium in the ratio (1/0.2) is marked in red. Measurement real-time was 30 s. (For interpretation of the references to color in this figure caption, the reader is referred to the web version of this article.)

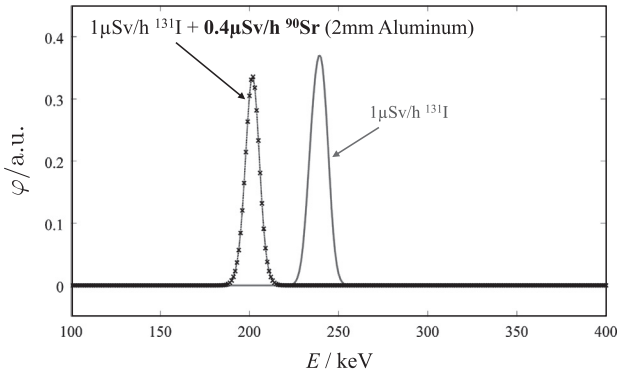

Fig. 8. Deconvolution of pure Iodine ^{131}I source in black compared with the deconvolution results of Strontium ^{90}Sr masked with ^{131}I in ratios (1/1), (1/0.5) and (1/0.2). $N=500$ iterations were used in the process.

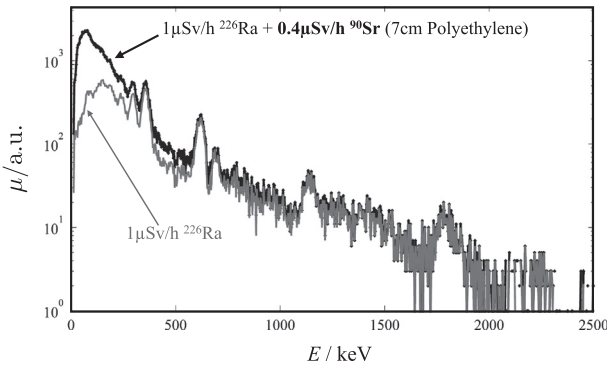

Fig. 9. ^{226}Ra spectra yielding the pure source in black and the source with additional strontium in the same ratios as used before plotted in red. Measurement real-time was 30 s. (For interpretation of the references to color in this figure caption, the reader is referred to the web version of this article.)

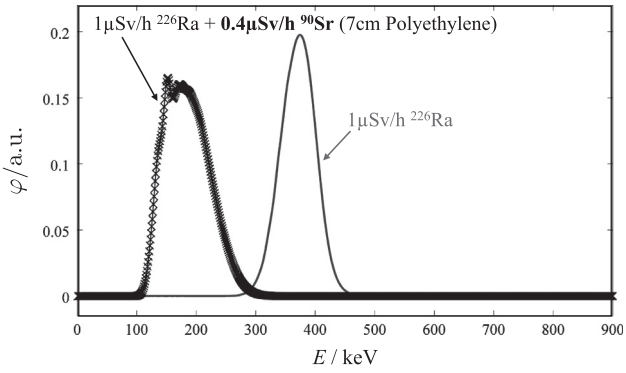

Fig. 10. Deconvolution of pure radium ^{226}Ra spectrum in black compared with the deconvolution results of strontium ^{90}Sr masked with ^{226}Ra in ratios (1/1), (1/0.5) and (1/0.2). $N=500$ iterations were used in the process.

caused by a 14 cm polyethylene shielding. In this case, the strontium source was shielded with 2 cm aluminum.

The ^{90}Sr effect results in a shifted peak position and we see a qualitative difference in the shape of the peak with and without the strontium. The deconvolved peak with strontium is narrower than the peak without it. Both the full width at half maximimum (FWHM) and the position can be regarded as the criteria for an identification procedure.

4.3. Masking with the multi-peak source ^{226}Ra

Radium ^{226}Ra is a decay product of the natural decay chains and also a NORM material. This source features multiple peaks and typically the identification of a threat that is masked by radium is rather elaborated. For the same dose rates as before, the results for this case are given in Figs. 9 and 10. Our masking source was lightly shielded with cadmium.

The deconvolved peak of ^{226}Ra is much broader than in the previous examples and the presence of strontium yields a considerable difference to the bare ^{226}Ra source.

5. Identification procedure

5.1. Blind identification

Based on our experiences with the deconvolution technique, we can straightforwardly formulate an identification algorithm. We refer to this option as blind identification, as the masking source is not expected to be known, yet. The presence of ^{90}Sr when measured with a common sodium iodide γ detector is clearly indicated by the location of the deconvolution peak. It is our primary criterion and although we have seen that this peak tends to shift towards higher channel numbers (see ^{131}I test results) for strong scattering, it never left a certain region from channel 140 to channel 230.

In our case, we decided to keep the actual ID as short as possible and implemented a simple region-of-interest (as stated before, from channel 140 to channel 230) together with a threshold value for the counts in the interest window.

Fig. 11 shows the result of our present indication for a strontium source masked by ^{40}K. A safe value for the identification threshold was assumed and a limiting ratio of approximately 1/10 was found for the case of blind identification. For better impression about the spreading of the pure results, we also included the results for iodine and radium in the figure. Similar results are obtained with the other masking combinations.

5.2. Combinatorial identification

The combinatorial identification makes use of an identification prestage. In this separate algorithm, the identity of possible masking sources is determined prior to the deconvolution. Once, this identity is known, the thresholds for the deconvolution peak of strontium can be adapted accordingly. There are various techniques to implement such adaptive processing and our solution will be covered by a different paper in more detail, so we will just briefly describe the idea.

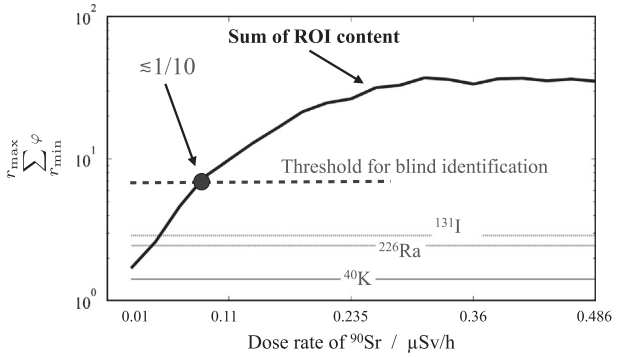

Fig. 11. Content of the ROI from $r_{min}=140$ to $r_{max}=230$ for the deconvolution of strontium masked by ^{40}K. The static values for pure iodine, potassium and radium are shown as comparison. A threshold was defined so that a masking ratio of 1 part strontium and 10 parts potassium can be resolved. $N=500$ iterations were used in the deconvolution.

As one can see from Fig. 11 the threshold for the strontium ID could be lower, if it is e.g. known that the masking source is potassium. The threshold could be adjusted even lower than the value reached when iodine is present, as iodine was ruled out by the pre-identification. Using pattern matching neural network (perceptron) that is trained with large databases of test spectra, it is possible to determine the primary isotope in the spectrum. As with the most modern algorithms for nuclide identification, the task to find this first, dominant nuclide is rather reliable. It is far more difficult to extract the presence of additional or multiple weak sources. With the knowledge of the masking nuclide, the decision threshold for the deconvolution peak becomes adaptive and can be chosen in dependency of the mask. This secondary step is performed by another neural net, specifically trained using data sets with and without strontium.

6. Summary and outlook

We presented a method to extract the pattern of a ^{90}Sr source from a γ spectrum. Based on the analytical model for the β decay and its prediction for the emission distribution, we constructed a β^- response matrix for a sodium iodide detector. This matrix was used in a Maximum-Likelihood deconvolution algorithm to extract a unique feature from the β^- radiation. The deconvolution is stable and produces peaks even in the presence of nuisance or masking sources. We tested the procedure with different masking sources and found results that showed a good separation between the masking pattern and the strontium pattern.

The deconvolution peak can be used as decision criterion in simple blind identification algorithms or in more elaborated codes using prior analysis modules for the masking sources. For the blind identification case, the masking ratio for a safe threshold was deduced.

In future, we will present an identification code that intrinsically performs both matching and deconvolution. We will also extend our investigation to similar β^- emitters with different endpoint energies, like ^{204}Tl. Furthermore, we will mathematically study whether the deconvolution results feature attractor-like behaviour and stability.

Acknowledgments

Discussions with Y. Kong of FLIR Radiation GmbH. and G. Pausch of Oncoray and R. Arlt regarding response models, data interpretation and acquisition are gratefully acknowledged. H. Ghareeb provided some data and insights into challenges for modern food monitor concepts.

Table A1
List of materials together with their index number l and some physical properties.

Number (l)	Material	Thickness (mm)
1	Air	100
2	Water	50
3	Water	100
4	Human body matter	100
5	Polyethylene	30
6	Polyethylene	50
7	Aluminum	10
8	Aluminum	20
9	Aluminum	30

Appendix A. The absorption table

The table covers all materials used for the absorption and scattering description. It contains material base functions for air, water, human body tissue and polyethylene. Aluminum was added as a slightly stronger absorber to our considerations (Table A1).

References

[1] American National Standard Performance Criteria for Hand-held Instruments for the Detection and Identification of Radionuclides (ANSI N42.34).
[2] F.J. Bryant, A.C. Chamberlain, A. Morgan, G.S. Spicer, Radiostrontium Fall-out in Biological Materials in Britain, Technical Report AERE-HP/R 2056, AERE, Harwell, 1957.
[3] F.J. Bryant, A. Morgan, G.S. Spicer, The Determination of Radiostrontium in Biological Materials, Technical Report AERE-R 3030, AERE, Harwell, 1959.
[4] M.J. Owers, T.W. Evett, Analyst 89 (1967) 544.
[5] Categorization of Radioactive Sources, International Atomic Energy Agency (IAEA) Safety Standards Series (RS-G-1.9).
[6] E.A. Robinson, Predictive Decomposition of Time Series with Applications to Seismic Exploration, Ph.D. Thesis, MIT, 1954.
[7] L. Bouchet, Astronomy and Astrophysics Supplement Series 113 (1995) 167.
[8] L.J. Meng, D. Ramsden, IEEE Transactions on Nuclear Science NS-47 (2000) 1329.
[9] L. Butchins, J. Gosling, M. Hogbin, D. Jones, R. Lacey, J. Stearn, Is the holy grail plastic? Radiation identification from plastic scintillators, in: 2009 First International Conference on Advancements in Nuclear Instrumentation Measurement Methods and their Applications (ANIMMA), June 2009, pp. 1–4. http://dx.doi.org/10.1109/ANIMMA.2009.5503783.
[10] M. Rawool-Sullivan, R.J. Estep, D. Miko, Estimation of obliquely scattered gamma-ray response functions in the gross-count tomographic gamma scanner (GC-TGS) method, in: Nuclear Science Symposium Conference Record, Albuquerque NM, 1997.
[11] S.J. Wilderman, J.A. Fessler, N.H. Clinthorne, J.W. LeBlanc, W.L. Rogers, IEEE Transactions on Nuclear Science NS-48 (1) (2001) 111.
[12] C.-M. Herbach, Y. Kong, R. Lentering, M. Neuer, G. Pausch, C. Plettner, K. Ruhnau, J. Stein, A technique for estimating detection limits of radionuclide identifying detectors by means of computer simulations, in: Nuclear Science Symposium Conference Record, NSS '08, October 2008, IEEE. pp. 648–655. http://dx.doi.org/10.1109/NSSMIC.2008.4775218.
[13] S. Agostinelli, J. Allison, K. Amako, et al., Nuclear Instruments and Methods in Physics Research Section A: Accelerators, Spectrometers, Detectors and Associated Equipment 506 (3) (2003) 250, http://dx.doi.org/10.1016/S0168-9002(03)01368-8.
[14] R.J. Estep, M. Rawool-Sullivan, D. Miko, IEEE Transactions on Nuclear Science NS-45 (1998) 1022.
[15] M. Rawool-Sullivan, R.J. Estep, M.W. Johnson, W. Murray, IEEE Transactions on Nuclear Science NS-47 (2000) 1395.
[16] K. Römer, G. Pausch, K. Saucke, Simulation of template spectra for scintillator based radionuclide identification devices using Geant4, in: IEEE Nuclear Science Symposium Conference Record, San Diego, CA, 2006. pp. 247–252.
[17] M.J. Neuer, K. Ruhnau, A. Ruhnau, R. Lentering, G. Pausch, F. Platte, J. Stein, Surveillance of nuclear threats using multiple, autonomous detection units, in: Nuclear Science Symposium Conference Record, NSS '08, October 2008, IEEE. pp. 3324–3329. http://dx.doi.org/10.1109/NSSMIC.2008.4775056.

[18] C.R. Subrahmanya, Astronomy and Astrophysics 89 (1980) 132.
[19] S.H. Suyu, P.J. Marshall, M.P. Hobson, R.D. Blandford, Monthly Notices of the Royal Astronomical Society (2007) 1.
[20] L.A. Shepp, Y. Vardi, Maximum likelihood reconstruction for emission tomography, in: IEEE Transactions on Medical Imaging, MI1 2, 1982.
[21] K. Krane, D. Halliday, Introductory Nuclear Physics, Wiley, 1987.
[22] R. Arlt, K. Baird, J. Blackadar, C. Blessenger, D. Blumenthal, P. Chiaro, K. Frame, E. Mark, M. Mayorov, M. Milodov, R. York, Semi-empirical approach for performance evaluation of radionuclide identifiers, in: Proceedings of the IEEE Nuclear Science Symposium, Orlando, USA, 2009.